

Chiral superconductivity near a fractional Chern insulator

Taige Wang¹ and Michael P. Zaletel¹

¹*Department of Physics, University of California, Berkeley, CA 94720, USA*

Superconductivity arising from fully spin-polarized, repulsively interacting electrons can host intrinsically chiral Cooper pairs and Majorana zero modes, yet no concrete microscopic route to such a state has been established. Motivated by recent observations in twisted MoTe₂ and rhombohedral pentalayer graphene, where fractional Chern insulators (FCIs) appear adjacent to spin-valley-polarized superconductors, we investigate a minimal model: spinless electrons in the lowest Landau level subject to a tunable moiré potential. Large-scale density-matrix renormalization group (DMRG) calculations show that, as the FCI gap closes, two nearly degenerate phases emerge before a metallic state forms. A chiral $f + if$ superconductor and a commensurate $\sqrt{3} \times \sqrt{3}$ charge-density wave (CDW) differ in energy by less than 1%, reproducing the distinct superconducting and re-entrant integer quantum Hall (RIQH) phases experimentally observed near the FCI regime. The superconducting dome remains robust against realistic Coulomb screening, light doping, and variations in lattice geometry. Melting the FCI therefore provides a new mechanism for realizing spin-polarized chiral superconductivity and RIQH order. We predict that twisted MoTe₂ at larger twist angles will develop a superconducting dome even at filling $\nu = 2/3$, and suppressing this superconductivity with a magnetic field should drive the system into an RIQH state.

INTRODUCTION

Few quantum states promise as much scientific insight and technological leverage as superconductivity. In conventional metals phonons bind electrons into singlet Cooper pairs [1]; in correlated oxides antiferromagnetic magnons have been argued to play the same role, as suggested by neutron resonance data and Hubbard-model calculations [2, 3]. Removing one spin species eliminates both glues and raises a fundamental question: *Can a purely repulsive, fully spin-polarized electron fluid still form a superconductor?* An affirmative answer would be significant, because any such condensate is expected to be *chiral* and might host Majorana modes [4, 5].

Two-dimensional moiré materials have placed this puzzle on experimental footing. Twisted MoTe₂ bilayers and rhombohedral pentalayer graphene realize ultra-flat, spin-polarized Chern bands. At filling $|\nu| = 2/3$ they stabilize a fractional Chern insulator (FCI) [6–10]. Yet modest doping in MoTe₂ or weakening the moiré in rhombohedral graphene collapses the FCI and unveils a spin-valley-polarized superconductor—despite the absence of any obvious pairing glue [11, 12]. Weak-coupling theories hint at triplet instabilities, but their assumptions fail in the strongly correlated regime experimentally probed [13–18].

Here we propose a minimal model that explains how an FCI can melt into *either* of two competing descendants—a spin-polarized chiral superconductor (SC) or a re-entrant integer quantum Hall (RIQH) phase. Our minimal model treats spinless electrons confined to the lowest Landau level and subject to a tunable periodic potential, capturing the key ingredients of twisted MoTe₂ and related moiré systems: a single, nearly “ideal Chern band” with adjustable bandwidth [19–22]. For spin-polarized Chern bands that support FCI, this model

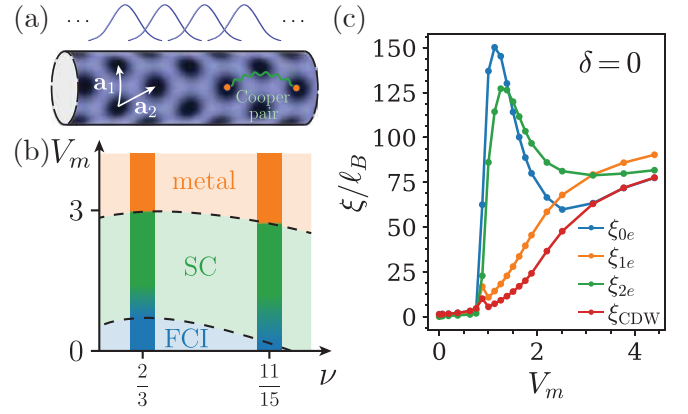


FIG. 1. Triangular-lattice LLL model and resulting phase diagram. (a) Infinite cylinder with spin-polarized LLL orbitals (schematic curves) and triangular lattice potential (color scale). Dark color denotes low potential and therefore high electron density. Vectors $\mathbf{a}_{1,2}$ define the YC lattice wrapping the cylinder. (b) Numerical phase diagram at $L_y = 5\ell_B$ and DMRG bond dimension $\chi = 10000$. A fractional Chern insulator (FCI, blue) and a compressible metal (orange) are separated by a dome of chiral superconductivity (green); dashed lines interpolate phase boundaries obtained at $\nu = 2/3$ and $11/15$. (c) Correlation lengths at $\nu = 2/3$ for the same cylinder and χ : neutral ξ_{0e} (blue), single-electron ξ_{1e} (orange), Cooper-pair ξ_{2e} (green), and density-wave ξ_{CDW} (purple) sectors are shown. The window $\xi_{2e} > \xi_{1e}$ signals Luther–Emery liquid behavior, while $\xi_{2e} > \xi_{0e}$ marks the quasi-1D superconducting regime.

plays a role analogous to the one-band Hubbard model for cuprates.

Large-scale infinite-cylinder density-matrix renormalization group (DMRG) yields the first non-perturbative evidence that a purely repulsive, fully spin-polarized fluid could condense into a superconducting state. As the Laughlin gap closes, the expected FCI–metal tran-

sition is pre-empted by two nearly degenerate descendants whose energies differ by less than 1%: (i) a dome of chiral f -wave superconductivity that evolves smoothly from tightly bound, BEC-like pairs on the FCI side to weak-coupling, BCS-like behavior on the metallic side, and (ii) a commensurate $\sqrt{3} \times \sqrt{3}$ charge-density wave carrying Hall conductance $\sigma_{xy} = 1$, mirroring the RIQH state observed experimentally by doping the FCI in both twisted MoTe₂ and rhombohedral pentalayer graphene [10, 11, 23]. Thus melting an FCI provides a unified microscopic mechanism for both spin-polarized chiral superconductivity and RIQH order in moiré Chern bands.

We outline a field-theoretic framework in which collapsing FCI can fuel *either* the chiral superconductor or the CDW—without recourse to dopant-induced anyon superconductivity [24]. Regardless of its microscopic origin, the pairing we find shows that the FCI-to-metal boundary is a promising place to look for spin-polarized superconductivity in Chern bands and gives us a simply model for studying this regime further. Two immediate experimental tests follow from our study. First, moving to larger twist angles beyond the narrow-band FCI limit should broaden the superconducting dome to encompass filling factor $\nu = 2/3$. Second, applying a magnetic field strong enough to quench the superconductivity should expose the closely competing re-entrant integer quantum Hall (RIQH) phase, as already observed in twisted MoTe₂ [11].

TRIANGULAR-LATTICE LLL MODEL

We study spin-polarized electrons confined to the lowest Landau level (LLL) on an infinite cylinder of circumference L_y as shown in Fig. 1(a). The particles interact via a two-body potential $V(\mathbf{q})$ and experience a triangular lattice potential of amplitude V_m ,

$$\hat{H} = \frac{1}{2} \sum_{\mathbf{q}} V(\mathbf{q}) \rho_{-\mathbf{q}} \rho_{\mathbf{q}} - V_m \sum_j \rho_{\mathbf{G}_j}, \quad (1)$$

where $\rho_{\mathbf{q}}$ is the bare density operator and $\{\mathbf{G}_j\}$ are the six shortest reciprocal-lattice vectors. The lattice constant a of the triangular lattice is chosen so that there is one flux quantum per-unit cell, $\frac{\sqrt{3}}{2}a^2 = 2\pi\ell_B^2$, resulting in a single $C = 1$ Chern band without Hofstadter subbands. The lowest Landau level (LLL) projected single-particle dispersion is

$$\epsilon_{\mathbf{k}} = 2V_m e^{-\frac{\pi}{\sqrt{3}}} \sum_{j=1}^3 \cos(\mathbf{k} \cdot \mathbf{a}_j) \quad (2)$$

where $\mathbf{a}_{1,2,3}$ are the Bravais vectors shown in Fig. 1(a) with $\mathbf{a}_3 = \mathbf{a}_2 - \mathbf{a}_1$. This model preserves the triangular symmetry of twisted MoTe₂ and rhombohedral

pentalayer graphene while imposing an *ideal* band geometry, i.e., strictly uniform Berry curvature and a vanishing trace condition [19, 20]. In the actual materials these quantum-geometric quantities deviate rather weakly from the ideal limit [21, 22], so the simplified Hamiltonian captures the essential physics. We note our model has in addition a C_2 symmetry, which these valley-polarized materials do not.

After projection to the LLL, ground states are obtained with infinite-cylinder DMRG that conserves the global $U(1)$ charge and the momentum k_y [25, 26]. Unless stated otherwise we use a pure contact repulsion $V(\mathbf{r}) = 4\pi\ell_B^2 \nabla^2 \delta(\mathbf{r})$ (Haldane pseudopotential $V_1 = 1$) [27] and impose “YC” boundary conditions, i.e., one in which triangular Bravais vector $\mathbf{a}_1 = (0, a)$ wraps around the cylinder. Circumferences $L_y = 4a - 9a$ are explored. The effect of a gate-screened Coulomb tail and of a square-lattice potential is analyzed at the end.

SUPERCONDUCTING DOME

We concentrate on fillings in the vicinity of the $\nu = 2/3$ Laughlin state and define the doping $\delta \equiv \nu - \frac{2}{3}$; fillings near $\nu = 1/3$ yield an analogous phase diagram (see Supplementary Material). Fig. 1(b) presents the numerical phase diagram as a function of lattice amplitude V_m for a cylinder of circumference $L_y = 5\ell_B$. Phase boundaries are determined from the correlation lengths of four quantum number sectors: the neutral sector ξ_{0e} , the single-electron sector ξ_{1e} , the Cooper-pair sector ξ_{2e} , and the density-wave sector ξ_{CDW} (Fig. 1(c)). The first three carry momentum $k_y = 0$ with charges $0, e$, and $2e$, respectively, whereas the density-wave sector is charge neutral but carries finite k_y .

At $\delta = 0$ the two extremes of V_m behave as expected. For $V_m = 0$ the model reduces to the parent $\nu = 2/3$ Hamiltonian [27]; all ξ ’s remain short and the entanglement spectrum exhibits the $(1, 1, 2, 3, \dots)$ counting, confirming a gapped fractional Chern insulator (FCI, blue). At large V_m the kinetic energy dominates, a Fermi surface emerges (Fig. 3(b)), ξ_{1e} surpasses every other correlation length, and the ground state is a compressible metal (orange) [28].

The most striking feature is a broad *superconducting dome* that wedges itself between the topologically ordered FCI and the compressible metal. As soon as the Laughlin gap closes, the Cooper-pair length overtakes the single-electron length, $\xi_{2e} > \xi_{1e}$, signaling a Luther–Emery (LE) liquid in which single electrons are gapped while pair correlations decay algebraically [29, 30]. At the dome center ξ_{2e} reaches nearly ten cylinder circumferences and, within a narrower window, even exceeds the neutral length, $\xi_{2e} > \xi_{0e}$, marking a quasi-1D superconducting regime (green band in Fig. 1(b)). On wider cylinder $L_y = 7a$, this regime already spans most of

the LE phase (see Supplementary Material), suggesting that pairing correlations will only grow as the system approaches two dimensions.

Electron doping to $\delta = 1/15$ ($\nu = 11/15$) preserves the same three-phase sequence: an FCI at small V_m , a superconducting dome at intermediate V_m , and a metal at large V_m . Within the doped FCI the density-wave channel becomes longest, $\xi_{\text{CDW}} > \xi_{0e}$, indicating an incipient anyon Wigner crystal and pushing the transition out of FCI to lower V_m (see Supplementary Material). Pairing is enhanced throughout compared to at $\nu = 2/3$: ξ_{2e} exceeds its undoped value across the dome. The hole-doped case $\delta = -1/15$ is omitted because it realizes a distinct $\nu = 3/5$ Jain state.

The close similarity of the $\delta = 0$ and $\delta = 1/15$ phase diagrams shows that superconductivity arises from the melting of the parent FCI itself, not from dopant-induced quantum-Hall fluids—thereby disfavoring “anyon superconductivity” mechanism that require a separate Hall state of the dopants [24, 31–34].

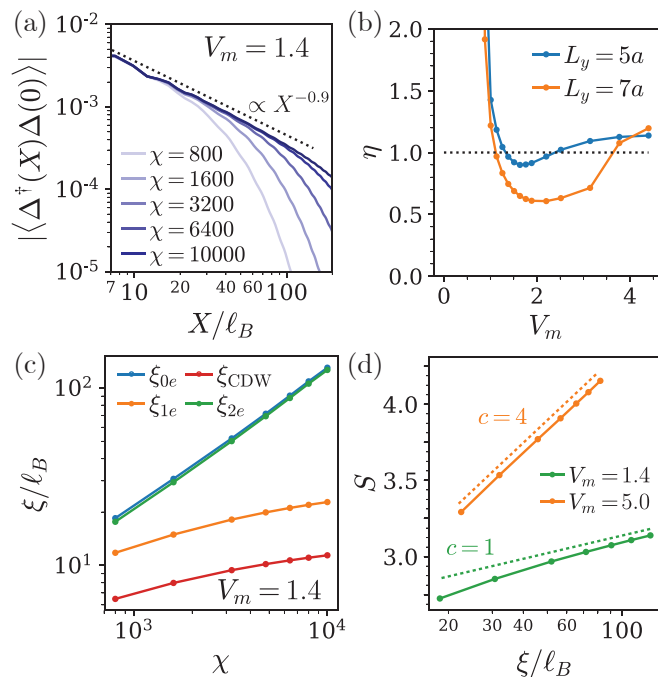


FIG. 2. Luther–Emery liquid inside the superconducting dome at $\nu = 2/3$. (a) Pair correlator $|\langle \Delta^\dagger(X)\Delta(0) \rangle|$ at $V_m = 1.4$ and $L_y = 5a$ for increasing bond dimension χ . A power-law decay $X^{-\eta}$ with $\eta \simeq 0.9$ confirms algebraic long-range order of the superconductivity. (b) Luttinger exponent η versus lattice amplitude V_m for $L_y = 5a$ (blue) and $L_y = 7a$ (orange). (c) Correlation lengths at $V_m = 1.4$ and $L_y = 5a$ as a function of χ . (d) Entanglement entropy S versus correlation length ξ tuned by χ . A log–linear fit gives central charge $c \simeq 1$ in the superconducting dome ($V_m = 1.4$, green) and $c \simeq 4$ in the metallic phase ($V_m = 5.0$, orange).

LUTHER–EMERY LIQUID

On an infinite cylinder the system is effectively one-dimensional, so a continuous $U(1)$ symmetry cannot break and the Cooper pair field satisfies $\langle \Delta \rangle = 0$. Superconductivity must therefore manifest as a Luther–Emery (LE) liquid [29, 30]: single electrons are gapped, whereas Cooper pairs remain gapless. Consequently the single-electron Green’s function decays exponentially, $|\langle c^\dagger(X)c(0) \rangle| \propto e^{-X/\xi_{1e}}$, while the pair correlator shows algebraic order $|\langle \Delta^\dagger(X)\Delta(0) \rangle| \propto X^{-\eta}$. The Luttinger exponent η sets the dominant tendency: $\eta < 1$ favors superconductivity, $\eta > 1$ favors charge density wave [35, 36].

To investigate this decay numerically we note that the specific real-space shape of the pair field Δ on the cylinder does not influence the asymptotic scaling of its correlations for separations $X \gg L_y$ along the cylinder axis. We therefore adopt a definition that is convenient for our MPS simulations. In Landau gauge the single-particle orbitals are labeled by their transverse momentum $k_y = 2\pi j/L_y$ with $j \in \mathbb{Z}$. For Fig. 2(a) we define the pair operator

$$\Delta(X) = c_{i+X}^\dagger c_{j+X}^\dagger, \quad (3)$$

where (i, j) specifies the pair and the separation X is taken in integer multiples of L_y/a . The correlations are strongest when $i + j \equiv 0 \pmod{L_y/a}$, indicating zero-momentum pairing ($k_y = 0$). Throughout the superconducting dome the pair correlator follows a power law over nearly two decades in distance, while the single-electron correlator decays exponentially (see Supplementary Material), confirming gapped quasiparticles but gapless Cooper pairs. A finite interval in V_m satisfies $\eta < 1$ Fig. 2(b). This interval widens and η decreases when the circumference is increased from $L_y = 5a$ to $7a$, indicating that pairing correlations strengthen as the system approaches two dimensions.

Correlation lengths and the central charge provide additional evidence for the LE liquid phase. As the bond dimension χ grows, ξ_{1e} saturates but $\xi_{2e} \propto \chi^\kappa$ diverges with a power-law in χ , and fits of the entanglement entropy $S = (c/6) \ln \xi + \text{const}$ yield a central charge $c \simeq 1$ inside the dome—consistent with a single gapless Goldstone mode. Outside the dome, where the Fermi surface intersects four momentum wires at $L_y = 5a$ (Fig. 3(b)), the same analysis gives $c \simeq 4$, as expected.

The simultaneous observation of algebraic pair order, divergent ξ_{2e} alongside a saturated ξ_{1e} , and a central charge $c \simeq 1$ unequivocally identifies the entire superconducting dome as a LE liquid phase on the $L_y = 5a, 7a$ cylinder. The decrease in η with system size suggests that the superconducting dome will evolve smoothly into a superconductor in the two-dimensional limit.

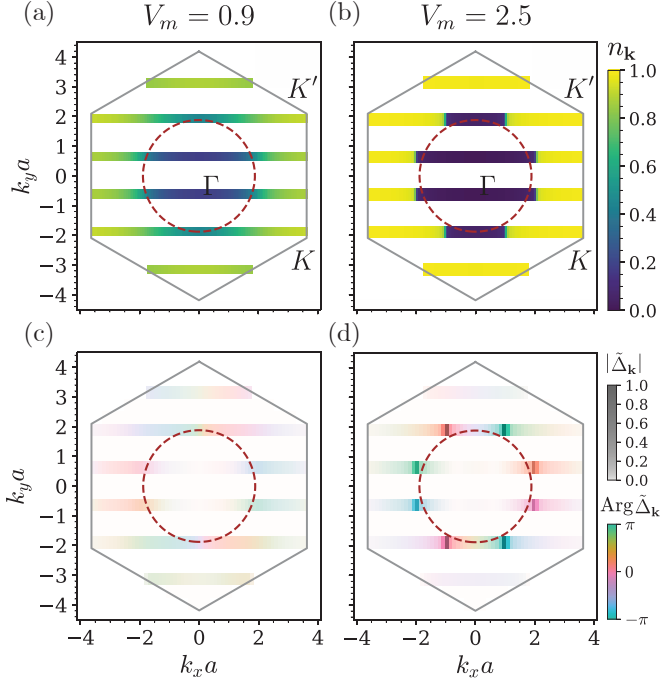


FIG. 3. **Momentum-space structure of the chiral f -wave pairing state.** (a,b) Single-particle occupation $n_{\mathbf{k}}$ in the Brillouin zone (grey hexagon) for lattice amplitudes $V_m = 0.9$ (left, FCI side of the dome) and $V_m = 2.5$ (right, metallic side). Horizontal strips mark the allowed k_y values on the $L_y = 5a$ cylinder; red dashed contour marks the non-interacting Fermi surface. Steps in $n_{\mathbf{k}}$ marks the Fermi surface. (c,d) Magnitude (greyscale) and phase (hue) of the proxy gap function $\tilde{\Delta}_{\mathbf{k}}$ for the same two values of V_m . In both cases the phase winds by 6π around the Fermi pocket, characteristic of chiral $f + if$ pairing ($C_{\text{BdG}} = 5$ due to parent Chern band).

PAIRING SYMMETRY AND THE BEC–BCS CROSSOVER

Identifying the pairing symmetry is pivotal for any unconventional superconductor. It can be probed by phase-sensitive experiments, benchmarked against analytic theory, and dictates the BdG Chern number—and therefore the count of chiral Majorana modes. Because $\langle \Delta \rangle = 0$ on the cylinder, we turn to the leading long-range charge- $2e$ fluctuation. Diagonalizing the MPS transfer matrix in that sector yields an eigenvector v that defines a non-local pair operator Δ_v whose correlator decays slowest with distance. Consistent with zero-momentum pairing, the associated eigenvalue is found to be real. Correlating Δ_v with a local pair $\Delta_{ij} = \langle c_i^\dagger c_j^\dagger \Delta_v \rangle$ (see Supplementary Material for details), and Fourier transform produces a momentum-resolved proxy gap function $\tilde{\Delta}_{\mathbf{k}} \propto \langle c_{-\mathbf{k}} c_{\mathbf{k}} \rangle_v$.

To analyze our results in momentum space, we introduce magnetic Bloch states $|\mathbf{k}\rangle$, defined as simultaneous eigenstates of the magnetic translation operators T_1 and T_2 . The magnetic translation algebra enforces the point-

group action $C_6 |\mathbf{k}\rangle = |C_6 \mathbf{k}\rangle$ on a cylindrical geometry imposes the quantization condition $e^{ik_y L_y} = (-1)^{L_y/a}$ (see Supplementary Material for details). Consequently, for circumferences $L_y = 5a$ in Fig. 3, the allowed k_y values exclude the origin at $k_y = 0$.

Throughout the dome the phase of $\tilde{\Delta}_{\mathbf{k}}$ winds by 6π around the Γ pocket (Fig. 3(c,d)), signaling chiral $f + if$ pairing. In a normal-state Chern band with Chern number $C = 1$, the Bogoliubov–de Gennes Chern number obeys $C_{\text{BdG}} = 2C + \ell$ [37, 38]. Taking $\ell = 3$ yields $C_{\text{BdG}} = 5$ and hence $c_- = 5/2$, so the superconducting phase hosts five co-propagating Majorana edge modes. The entire dome therefore corresponds to a single chiral $f + if$ phase, presenting a sharp observable for phase-sensitive probes such as Josephson interferometry or quasiparticle-interference imaging.

The proxy gap function evolves smoothly from the strong coupling side to the weak coupling side. On the FCI side the amplitude of $\tilde{\Delta}_{\mathbf{k}}$ is nearly uniform and the single-particle occupation $n_{\mathbf{k}}$ varies gently across the Brillouin zone, indicating tightly bound bosonic pairs—a BEC-like regime (Fig. 3(a,c)). Closer to the metallic edge, $n_{\mathbf{k}}$ develops sharp steps at the non-interacting Fermi contour, and $\tilde{\Delta}_{\mathbf{k}}$ concentrates on these crossings (Fig. 3(b,d)), hallmarks of weak-coupling, Fermi-surface pairing. Because the correlation lengths evolve smoothly across this range (Fig. 1), the dome realizes a continuous BEC–BCS crossover: tightly bound pairs on the insulating flank morph into weak-coupling Cooper pairs near the metal without any intervening phase transition or change in the topological character.

COMPETING INSTABILITIES AND ROBUSTNESS OF THE SUPERCONDUCTIVITY

Within the triangular-lattice LLL model we find two phases compete closely with the chiral superconductor: a compressible Luttinger metal and a commensurate $\sqrt{3} \times \sqrt{3}$ charge-density wave (CDW), where the latter is also a re-entrant integer quantum Hall (RIQH) state (i.e. $\sigma_{xy} = e^2/h$ at $\nu = 2/3$). Table I summarizes the ground state at each cylinder circumference explored, and Fig. 4(a) presents the corresponding energies.

| L_y/a | Geometric feature | Ground state |
|---------|---|---------------------|
| 5, 7 | APBC | Superconductor (SC) |
| 4, 8 | PBC, solitary wire $k_y = 0$ | Partially-gapped SC |
| 6, 9 | $\sqrt{3} \times \sqrt{3}$ commensurate | CDW (RIQH) |

TABLE I. Geometric effect that selects the ground state at different circumferences, examined inside the superconducting dome identified at $L_y = 5a$.

Even-odd effects familiar from Hubbard ladders [39–41] also control our spin-polarized cylinders. Our band

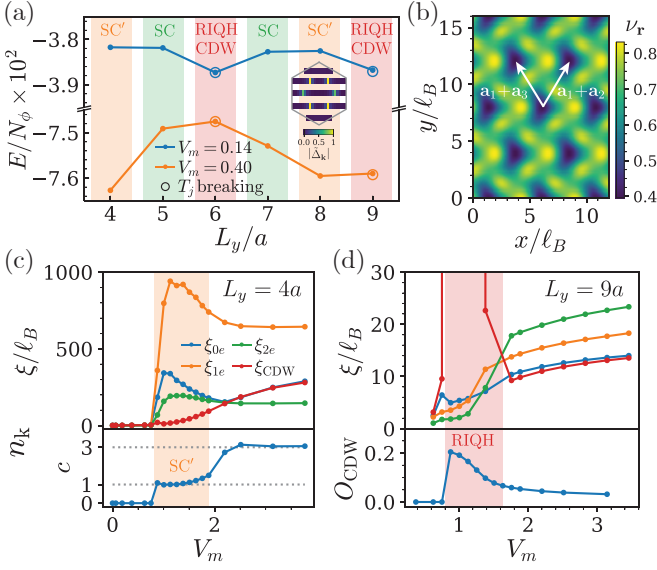


FIG. 4. **Competing instabilities.** (a) Ground-state energy per flux quantum E/N_Φ , versus cylinder circumference L_y for two lattice amplitudes. Background shading identifies the phase inferred at each L_y : partially-gapped superconductor (SC', orange), superconductor (SC, green), and charge-density wave (CDW, RIQH, red). Open symbols denote runs in which translation symmetry is explicitly relaxed to favor a $\sqrt{3} \times \sqrt{3}$ CDW. Inset shows the proxy gap function $|\tilde{\Delta}_{\mathbf{k}}|$ of SC'. (b) Real-space filling factor $\nu_r(\mathbf{r})$ for the $\sqrt{3} \times \sqrt{3}$ CDW obtained at $V_m = 0.18$ on a $L_y = 6a$ cylinder. White arrows indicate the enlarged Bravais vectors. (c) Phase diagram for a $L_y = 4a$ cylinder. Top: correlation lengths in several sectors. Bottom: central charge c . The dotted lines are for visual guidance at $c = 1$ and 3 . The shaded window marks SC'. (d) Phase diagram for a $L_y = 9a$ cylinder. Top: correlation lengths from calculations that enforce translation symmetry. Inside the shaded re-entrant integer quantum Hall (RIQH) window ξ_{CDW} diverges. Bottom: CDW order parameter O_{CDW} from runs that allow translation breaking.

structure always features a completely filled $k_y = \pi$ wire, while the only partially filled self-conjugate wire is $k_y = 0$ (Fig. 3(b)). Due to the magnetic Bloch states $|\mathbf{k}\rangle$ we choose, the system switches between periodic (PBC) and antiperiodic (APBC) boundary conditions as the cylinder alternates between even and odd circumference (see Fig. 3 and Supplementary Material). For even circumferences $L_y = 4a$ and $8a$ that wire is unpaired. Josephson couplings can gap neighboring wires pairwise, but a solitary wire is hard to be phase-locked and forces a Luttinger liquid. At $L_y = 4a$, Fig. 4(c) reveals an intermediate window where $\xi_{1e} > \xi_{2e}$ yet the entropy collapses to central charge $c \approx 1$, far below the $c = 3$ expected from three gapless wires. We interpret the state as a partially gapped superconductor (SC'): the $k_y = 0$ wire remains gapless, whereas the other two wires form a Luther–Emery (LE) liquid. This conclusion is supported by the proxy gap function $\tilde{\Delta}_{\mathbf{k}}$ plotted in the inset of Fig. 4(a), where the gap along the $k_y = 0$

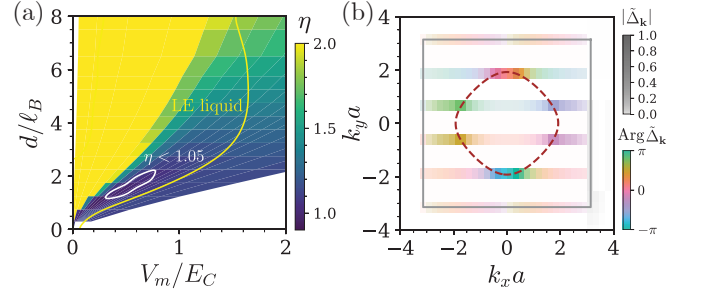


FIG. 5. **Robustness of the superconducting dome.** (a) Luttinger exponent η on a $L_y = 5a$ cylinder as a function of lattice amplitude V_m and gate distance d for a screened Coulomb interaction. The yellow curve encloses the Luther–Emery (LE) liquid where $\xi_{2e} > \xi_{1e}$, while the inner white contour highlights the region with $\eta < 1.05$. (b) Momentum-resolved proxy gap function $\tilde{\Delta}_{\mathbf{k}}$ for a square-lattice potential at filling $\nu = 11/15$ and $V_m = 0.4$ on a $L_y = 5a$ cylinder. The phase retains the 6π winding similar to the triangular lattice case.

wire is exceptionally small. Finite bond dimension underestimates this weak Goldstone mode, so DMRG captures only the most mobile single-electron sector and yield $c \approx 1$ rather than the ideal $c = 2$. For odd circumferences $L_y = 5a$ and $7a$ every wire has a partner, all charge modes lock coherently, and a LE superconductor results. This obstruction is a quasi-1D artifact: a single momentum wire occupies a vanishing fraction of the Brillouin zone, so it should not hinder superconductivity in the thermodynamic limit.

A more consequential competitor is the commensurate $\sqrt{3} \times \sqrt{3}$ charge-density wave (CDW) [42–45], which emerges whenever the cylinder circumference matches an integer multiple of its enlarged unit cell, i.e. $L_y = 6a$ or $9a$. In translation-symmetric DMRG runs the ground state is forced into an equal superposition of the three translated CDW patterns, producing a diverging correlation length ξ_{CDW} (Fig. 4(d)). Once translation symmetry is relaxed the wavefunction settles into the pattern of Fig. 5(b): every $\sqrt{3} \times \sqrt{3}$ plaquette hosts exactly one unit of excess (hole) charge. The state is insulating with no gapless charge modes, and charge-pumping diagnostics confirm a quantized Hall response $\sigma_{xy} = e^2/h$ (see Supplementary Material), firmly identifying it as a re-entrant integer quantum Hall (RIQH) phase. Comparable RIQH states are observed on the electron-doped side of twisted MoTe_2 [11] and in doped pentagonal graphene [10, 12, 23], whereas superconductivity appears on the hole-doped side or when the moiré potential is weakened—mirroring the delicate balance we uncover numerically.

The competition between superconductivity and the CDW is razor-thin: at $V_m = 0.14$ (on the FCI flank) the $L_y = 6a$ CDW undercuts the superconducting cylinders at $L_y = 5a, 7a$ by less than 1%, whereas at

$V_m = 0.40$ (closer to the metal) the ordering reverses (Fig. 4(a)). The splitting is minuscule, well within finite-size error bars that leaves the two phases practically degenerate in our numerical calculation. For $L_y = 9a$ the translation-symmetric data trace an apparent sequence FCI \rightarrow CDW \rightarrow SC \rightarrow metal, but when symmetry is relaxed the charge-order parameter O_{CDW} remains finite across the entire window, hinting that density order and pairing may even coexist (Fig. 4(d)). Given such a tiny energy difference we cannot, at present, determine whether the true two-dimensional ground state at $\nu = 2/3$ is the chiral superconductor, the $\sqrt{3} \times \sqrt{3}$ CDW, or a phase intertwining the two; substantially larger system sizes will be required to settle the question. However, this near-degeneracy dovetails with experiment, where superconducting and RIQH regions occupy adjacent slices of the phase diagram [10, 11, 23], and modest knobs—out-of-plane magnetic field, heterostrain, carrier doping, or changes in the moiré-potential strength—readily tilt the balance between them.

We next probe how a finite interaction range modifies the dome. Replacing the contact potential by a gated Coulomb form,

$$V(\mathbf{q}) = E_C \frac{\tanh(qd)}{q\ell_B} \quad (4)$$

interpolates smoothly from the δ -function limit $d \rightarrow 0$ to the unscreened $1/r$ tail. Because the leading Haldane pseudopotential V_1 grows with d , the metal–FCI boundary shifts to larger bandwidth V_m/E_C . Yet the qualitative structure survives: a superconducting dome still interposes between the FCI and the metal, and its interior remains a Luther–Emery (LE) liquid with algebraic pair correlations (see Supplementary Materials). As shown in Fig. 5(a), The LE liquid behavior survives $d \lesssim 10\ell_B$ and the Luttinger exponent η touches unity for $d \lesssim 2\ell_B$ on a $L_y = 5a$ cylinder.

This window matches experimental length scales. For a 3.8° twisted MoTe_2 bilayer, the moiré period $a_M \simeq 5.2$ nm yields effective $\ell_B \approx 1.9$ nm; hBN spacers of 10–30 nm correspond to $d/\ell_B \approx 5 - 15$, overlapping the LE liquid regime [11]. In hBN-aligned rhombohedral pentalayer graphene, $a_M \simeq 14$ nm gives $\ell_B \approx 5.2$ nm; gate distances of 20–40 nm translate to $d/\ell_B \approx 4 - 7$, squarely inside the superconducting regime [12].

Chiral pairing also survives a drastic change of lattice geometry. Replacing the triangular lattice by a square lattice leaves only a faint LE liquid window at the parent filling $\nu = 2/3$, but a modest electron doping to $\nu = 11/15$ dramatically enlarges the window (see Supplementary material). The momentum-resolved gap shown in Fig. 5(b) still exhibits a 6π phase winding, confirming that the $f + if$ order and the underlying mechanism are properties of the FCI melting itself rather than of any Fermi-surface details. Taken together,

the gated-Coulomb map and the square-lattice test establish that the chiral superconductivity we find is remarkably robust—persisting across realistic screening lengths, carrier densities, and even disparate lattice geometries.

DISCUSSION

Our numerical calculations demonstrate that a fully spin-polarized, repulsive electron fluid can pass directly from a fractional Chern insulator to a chiral superconductor at fixed filling. One possible interpretation of this result is through a parton construction $c = bf$. We place the bosonic parton b in a bosonic IQH state with Hall conductance $\sigma_{xy}^b = 2e^2/h$. At $\nu = 2/3$ Galilean invariance then forces the fermionic parton f to a $C_f = 1$ Landau level, reproducing the Jain FCI (see Supplementary material). More generally, the low-energy theory is captured by the Chern-Simons Lagrangian

$$\mathcal{L} = \frac{1}{4\pi} \beta^\top \sigma_x d\beta + \frac{1}{2\pi} \beta^\top d(A - a) + \frac{C_f}{4\pi} \alpha d\alpha + \frac{1}{2\pi} \alpha da \quad (5)$$

where σ_x is the K -matrix of the bosonic IQH sector, C_f is the Chern number of the f -parton band, and a is the emergent gauge field that binds the partons into the physical electron. Bandwidth tuning can instead invert the f band to Chern number $C_f = -2$. The bosonic and fermionic Chern-Simons terms then cancel, the emergent gauge field becomes gapless, resulting in a chiral superconductor with edge chiral central charge $c_- = -2$, obtained without external doping. It lands in the same topological class as the anyon-superconductivity state proposed in Ref. [24] and has similarities in spirit, but here arises from a simple band inversion rather than from dopants forming a separate Hall liquid. The accompanying critical theory is the QED₃–Chern–Simons fixed point that also governs bosonic Laughlin-to-superfluid transitions [46–48].

Magnetic translations at filling $\nu = 2/3$ force the Chern number C_f to change in multiples of three, so the $C_f = -2$ route naturally selects superconductivity unless the lattice enlarges. A spontaneous $\sqrt{3} \times \sqrt{3}$ reconstruction releases this constraint. Choosing $C_f = +2$ produces the re-entrant IQH CDW seen both in our numerics and experiments [10, 11, 23]. Setting $C_f = 0$ yields a $\sqrt{3} \times \sqrt{3}$ density wave without Hall response, a pattern reported at large displacement field in twisted MoTe_2 [6, 7, 44]. Thus the parton picture unifies the superconductor, the RIQH CDW, and the $\sigma_{xy} = 0$ CDW as proximate descendants of the same FCI, while a direct FCI–metal transition lacks any field theory description—explaining why our numerics and the experiments invariably find an intervening ordered phase.

Whether the $f + if$ condensate we extract truly coincides with the parton-derived phase remains unsettled.

In the weak-coupling limit of a spin-polarized superconductor the Bogoliubov–de Gennes Chern number obeys $C_{\text{BdG}} = \ell$ for angular-momentum channel ℓ [49, 50]. A weak-coupling $f + if$ state therefore carries edge chiral central charge $c_- = 5/2$, whereas the parton construction yields $c_- = -2$; the two phases differ by a number of chiral $p + ip$ Majorana modes. More broadly, spin-polarized superconductors are expected to have half-integer c_- in the BCS limit and integer c_- in the BEC limit, apparently precluding a smooth crossover [51]. Yet our numerics display a continuous BEC–to–BCS evolution, forcing one of two resolutions: (i) the $c_- = -2$ parton superconductor shed its extra Majorana before reaching the metal; (ii) the superconducting dome is adiabatically connected to the weak-coupling $f + if$ phase and will end through a first-order phase transition into the FCI phase. A direct numerical extraction of the edge chiral central charge will be required to decide between these scenarios.

A complementary, weak-coupling interpretation is that interactions near the FCI become effectively attractive at intermediate length scales. Very recent numerical calculations show that Laughlin anyons can themselves bind into charge- $2e/3$ composites and even Cooper pairs [52–54]. Inside a pristine fractional quantum Hall (FQH) state Cooper pairs remain dispersionless and therefore cannot condense, but the periodic potential in our model endows the low-energy Cooper pairs with kinetic energy. Once the Laughlin gap softens, these Cooper pairs may condense into the chiral superconductor we observe, providing a microscopic route fully compatible with weak-coupling expectations. Regardless of whether the superconductor emerges through a continuous FCI–to–SC transition or via an effective mid-range attraction among anyons, the bandwidth-driven instability uncovered here offers a generic, dopant-free pathway to spin-polarized chiral pairing and naturally accounts for its close rivalry with re-entrant Hall order in current moiré heterostructures.

These results translate into clear experimental expectations. Because the superconducting dome nucleates precisely where the Laughlin gap first closes, increasing the twist angle—and hence the ratio of moiré potential to Coulomb energy—should broaden the dome so that robust chiral pairing already appears at the bare filling $\nu = 2/3$, without the need for extra carriers or deliberate suppression of the moiré potential. Conversely, slight doping or any perturbation that weakens the periodic potential (pressure, displacement field, heterostrain) relaxes the commensuration condition that stabilizes the $\sqrt{3} \times \sqrt{3}$ charge–density wave, thereby tipping the balance toward superconductivity. A systematic sweep of twist angle and carrier density in twisted MoTe_2 and rhombohedral pentalayer graphene can therefore test the “melt-the-FCI” scenario and controllably navigate between the superconducting and re-entrant integer quantum Hall (RIQH) regimes of a spin-polarized Chern band.

A perpendicular magnetic field offers an orthogonal tuning knob. Once the field is strong enough to quench the superconducting condensate, the system is predicted to enter the competing RIQH phase, yielding a transition from zero resistance to a quantized Hall plateau with $\sigma_{xy} = 1$. Superconductivity is inherently sensitive to out-of-plane fields, whereas the orbital moment associated with the Hall response favors the RIQH state—this field-induced crossover has already been reported in twisted MoTe_2 devices [11]. Inside the RIQH regime, real-space probes such as scanning tunnelling microscopy (STM) should detect the anticipated $\sqrt{3} \times \sqrt{3}$ density modulation [55–57], providing a direct structural fingerprint of the charge-density wave (CDW) and a decisive test of the microscopic picture developed here.

Note added– During writing of this manuscript, we become aware of Ref. 58 and 59, which discuss a similar field-theory construction of bandwidth-tuned FCI to superconductor transition.

Acknowledgments. We are especially grateful to Ya-Hui Zhang for helpful discussions. We thank Zhihuan Dong for collaboration on a related project. We acknowledge Daniel Parker, Dung-Hai Lee, T. Senthil, Tianle Wang, Sian Yang for discussion. This work is supported by the Simons Collaboration on Ultra-Quantum Matter, which is a grant from the Simons Foundation (1151944, MZ). This research uses the Lawrence Livermore computational cluster provided by the Lawrence Berkeley National Laboratory (Supported by the U.S. Department of Energy, Office of Basic Energy Sciences under Contract No. DE-AC02-05-CH11231).

-
- [1] J. Bardeen, L. N. Cooper, and J. R. Schrieffer, Theory of superconductivity, *Physical Review* **108**, 1175 (1957).
 - [2] J. Rossat-Mignod, L. P. Regnault, C. Vettier, P. Bourges, P. Bulet, J. Bossy, J.-Y. Henry, and G. Lapertot, Neutron scattering study of the $\text{YBa}_2\text{Cu}_3\text{O}_{6+x}$ system, *Physica C* **185–189**, 86 (1991).
 - [3] D. J. Scalapino, The case for $d_{x^2-y^2}$ pairing in the cuprate superconductors, *Physics Reports* **250**, 329 (1995).
 - [4] L. Fu and C. L. Kane, Superconducting proximity effect and majorana fermions at the surface of a topological insulator, *Physical Review Letters* **100**, 096407 (2008).
 - [5] C. Nayak, S. H. Simon, A. Stern, M. Freedman, and S. D. Sarma, Non-abelian anyons and topological quantum computation, *Reviews of Modern Physics* **80**, 1083 (2008).
 - [6] J. Cai, E. Anderson, C. Wang, X. Zhang, X. Xu, *et al.*, Signatures of fractional quantum anomalous hall states in twisted MoTe_2 , *Nature* **622**, 63 (2023).
 - [7] H. Park, J. Cai, E. Anderson, Y. Zhang, X. Xu, *et al.*, Observation of fractionally quantized anomalous hall effect, *Nature* **622**, 74 (2023).
 - [8] Y. Zeng, Z. Xia, K. Kang, J. Zhu, K. F. Mak, J. Shan, *et al.*, Thermodynamic evidence of fractional chern insulator in moiré MoTe_2 , *Nature* **622**, 69 (2023).

- [9] F. Xu, Z. Sun, T. Jia, C. Liu, C. Li, Y. Gu, T. Li, *et al.*, Observation of integer and fractional quantum anomalous hall effects in twisted bilayer $MoTe_2$, *Physical Review X* **13**, 031037 (2023).
- [10] Z. Lu, T. Han, Y. Yao, A. P. Reddy, L. Ju, *et al.*, Fractional quantum anomalous hall effect in multilayer graphene, *Nature* **626**, 759 (2024).
- [11] F. Xu, Z. Sun, J. Li, C. Zheng, C. Xu, J. Gao, T. Jia, K. Watanabe, T. Taniguchi, B. Tong, L. Lu, J. Jia, Z. Shi, S. Jiang, Y. Zhang, Y. Zhang, S. Lei, X. Liu, and T. Li, Signatures of unconventional superconductivity near reentrant and fractional quantum anomalous hall insulators, arXiv (2025), cond-mat.mes-hall, 2504.06972.
- [12] T. Han, Z. Lu, Z. Hadjri, L. Ju, *et al.*, Signatures of chiral superconductivity in rhombohedral graphene, *Nature* 10.1038/s41586-025-09169-7 (2025), published online 22 May 2025.
- [13] M. Geier, M. Davydova, and L. Fu, Chiral and topological superconductivity in isospin polarized multilayer graphene, arXiv preprint arXiv:2409.13829 10.48550/arXiv.2409.13829 (2024), 2409.13829.
- [14] Y.-Z. Chou, J. Zhu, and S. D. Sarma, Intravalley spin-polarized superconductivity in rhombohedral tetralayer graphene, *Physical Review B* **111**, 174523 (2025), 2409.06701.
- [15] G. Parra-Martinez, A. Jimeno-Pozo, V. T. Phong, H. Sainz-Cruz, D. Kaplan, P. Emanuel, Y. Oreg, P. A. Pantaleon, J. A. Silva-Guillen, and F. Guinea, Band renormalization, quarter metals, and chiral superconductivity in rhombohedral tetralayer graphene, arXiv preprint arXiv:2502.19474 10.48550/arXiv.2502.19474 (2025), 2502.19474.
- [16] Y.-Q. Wang, Z.-Q. Gao, and H. Yang, Chiral superconductivity from a parent chern band and its non-abelian generalization, arXiv preprint arXiv:2410.05384 10.48550/arXiv.2410.05384 (2024), 2410.05384.
- [17] G. Shavit and J. Alicea, Quantum geometric kohn-luttinger superconductivity, *Physical Review Letters* **134**, 176001 (2025), 2411.05071.
- [18] C. Xu, N. Zou, N. Peshcherenko, A. Jahin, T. Li, S.-Z. Lin, and Y. Zhang, Chiral superconductivity from spin polarized chern band in twisted mote₂, arXiv preprint arXiv:2504.07082 10.48550/arXiv.2504.07082 (2025), 2504.07082.
- [19] P. J. Ledwith, A. Vishwanath, and E. Khalaf, Family of ideal chern flat bands with arbitrary chern number in chiral twisted graphene multilayers, *Physical Review Letters* **128**, 176404 (2022).
- [20] P. J. Ledwith, A. Vishwanath, and D. E. Parker, Vortexability: A unifying criterion for ideal fractional chern insulators, *Physical Review B* **108**, 205144 (2023).
- [21] J. Dong, J. Wang, P. J. Ledwith, A. Vishwanath, and D. E. Parker, Composite fermi liquid at zero magnetic field in twisted mote₂, *Physical Review Letters* **131**, 136502 (2023).
- [22] J. Dong, T. Wang, T. Wang, T. Soejima, M. P. Zaletel, A. Vishwanath, and D. E. Parker, Anomalous hall crystals in rhombohedral multilayer graphene. i. interaction-driven chern bands and fractional quantum hall states at zero magnetic field, *Physical Review Letters* **133**, 206503 (2024).
- [23] Z. Lu, T. Han, Y. Yao, Z. Hadjri, J. Yang, J. Seo, L. Shi, S. Ye, K. Watanabe, T. Taniguchi, and L. Ju, Extended quantum anomalous hall states in graphene/hbn moiré superlattices, *Nature* **637**, 1090 (2025).
- [24] Z. D. Shi and T. Senthil, Doping a fractional quantum anomalous hall insulator, arXiv (2024), cond-mat.str-el, 2409.20567.
- [25] M. P. Zaletel and R. S. K. Mong, Exact matrix product states for quantum hall wave functions, *Phys. Rev. B* **86**, 245305 (2012).
- [26] M. P. Zaletel, R. S. K. Mong, and F. Pollmann, Topological characterization of fractional quantum hall ground states from microscopic hamiltonians, *Phys. Rev. Lett.* **110**, 236801 (2013).
- [27] F. D. M. Haldane, Fractional quantization of the hall effect: A hierarchy of incompressible quantum fluid states, *Physical Review Letters* **51**, 605 (1983).
- [28] In the metal, the finite ξ_{1e} is an artifact of the finite MPS bond dimension χ used in our DMRG numerics; ξ_{1e} scales algebraically with χ .
- [29] A. Luther and V. J. Emery, Backward scattering in the one-dimensional electron gas, *Physical Review Letters* **33**, 589 (1974).
- [30] V. J. Emery, Theory of the quasi-one-dimensional electron gas with strong “on-site” interactions, *Physical Review B* **14**, 2989 (1976).
- [31] R. B. Laughlin, Superconducting ground state of noninteracting particles obeying fractional statistics, *Physical Review Letters* **60**, 2677 (1988).
- [32] R. B. Laughlin, The relationship between high-temperature superconductivity and the fractional quantum hall effect, *Science* **242**, 525 (1988).
- [33] B. I. Halperin, Anyon superconductivity, *Helv. Phys. Acta* **65**, 80 (1990).
- [34] M. P. A. Fisher and D.-H. Lee, Correspondence between two-dimensional anyons and superconductivity, *Phys. Rev. B* **43**, 130 (1991).
- [35] H.-C. Jiang and T. P. Devereaux, Superconductivity in the doped Hubbard model and its interplay with next-nearest hopping t' , *Science* **365**, 1424 (2019).
- [36] M. Troyer, H. Tsunetsugu, T. M. Rice, J. Riera, and E. Dagotto, Spin gap and superconductivity in the one-dimensional t-j model with coulomb repulsion, *Physical Review B* **48**, 4002 (1993).
- [37] X.-L. Qi, T. L. Hughes, and S.-C. Zhang, Chiral topological superconductor from a quantum anomalous hall state, *Phys. Rev. B* **82**, 184516 (2010).
- [38] J. Wang, B. Lian, and S.-C. Zhang, Chiral superconducting phase and majorana fermions from the quantum anomalous hall plateau transition, *Phys. Rev. B* **92**, 064520 (2015).
- [39] H.-H. Lin, L. Balents, and M. P. A. Fisher, Weak-coupling renormalization group and dmrg studies of spinful hubbard ladders, *Phys. Rev. B* **56**, 6569 (1997).
- [40] U. Ledermann, K. L. Hur, and T. M. Rice, Successive opening of the fermi surface in doped n -leg hubbard ladders, *Phys. Rev. B* **62**, 16383 (2000).
- [41] E. Orignac and T. Giamarchi, Effects of disorder on two coupled chains of strongly correlated fermions, *Phys. Rev. B* **56**, 7167 (1997).
- [42] S. A. Kivelson, D.-H. Lee, and S.-C. Zhang, Global phase diagram in the quantum hall effect, *Physical Review B* **46**, 2223 (1992).
- [43] X.-Y. Song, C.-M. Jian, L. Fu, and C. Xu, Intertwined fractional quantum anomalous hall states and charge density waves, arXiv (2023), arXiv:2310.11632 [cond-mat.str-el].

- [44] X.-Y. Song, Y.-H. Zhang, and T. Senthil, Phase transitions out of quantum hall states in moiré materials, *Phys. Rev. B* **109**, 085143 (2024).
- [45] H. Lu, H.-Q. Wu, B.-B. Chen, K. Sun, and Z. Y. Meng, Interaction-driven roton condensation in $c = 2/3$ fractional quantum anomalous hall state, *arXiv* (2024), *arXiv:2403.03258* [cond-mat.str-el].
- [46] M. Barkeshli and J. McGreevy, Continuous transition between fractional quantum hall and superfluid states, *Phys. Rev. B* **89**, 235116 (2014).
- [47] T. Wang, X. Song, M. P. Zaletel, and T. Senthil, Emergent q_{ed_3} at the bosonic Laughlin state to superfluid transition, to appear.
- [48] J. Y. Lee, C. Wang, M. P. Zaletel, A. Vishwanath, and Y.-C. He, Emergent multi-flavor q_{ed_3} at the plateau transition between fractional Chern insulators: Applications to graphene heterostructures, *Phys. Rev. X* **8**, 031015 (2018).
- [49] G. E. Volovik, On edge states in superconductors with time inversion symmetry breaking, *JETP Letters* **66**, 522 (1997).
- [50] N. Read and D. Green, Paired states of fermions in two dimensions with breaking of parity and time-reversal symmetries and the fractional quantum hall effect, *Physical Review B* **61**, 10267 (2000).
- [51] V. Gurarie and L. Radzihovsky, Resonantly paired fermionic superfluids, *Annals of Physics* **322**, 2 (2007).
- [52] Q. Xu, G. Ji, Y. Wang, H. Q. Trung, and B. Yang, Dynamics of clusters of anyons in fractional quantum hall fluids, *arXiv* (2025), *arXiv:2505.20257* [cond-mat.str-el].
- [53] M. Gattu and J. K. Jain, Molecular anyons in fractional quantum hall effect, *arXiv* (2025), *arXiv:2505.22782* [cond-mat.str-el].
- [54] T. Wang and M. P. Zaletel, Anyon binding in fractional quantum hall states, to appear.
- [55] Y. Jiang, X. Lai, K. Watanabe, T. Taniguchi, K. Haule, J. Mao, and E. Y. Andrei, Charge order and broken rotational symmetry in magic-angle twisted bilayer graphene, *Nature* **573**, 91 (2019).
- [56] A. Kerelsky, L. J. McGilly, D. M. Kennes, L. Xian, M. Yankowitz, S. Chen, K. Watanabe, T. Taniguchi, J. Hone, C. R. Dean, A. Rubio, and A. N. Pasupathy, Maximized electron interactions at the magic angle in twisted bilayer graphene, *Nature* **572**, 95 (2019).
- [57] Z. Li, L. Zhu, K. Watanabe, T. Taniguchi, S. Meng, and F. Wang, Generalized Wigner crystal states in graphene moiré superlattices, *Nature* **597**, 650 (2021).
- [58] Z. D. Shi and T. Senthil, Anyon delocalization transitions out of a disordered fqah insulator, *arXiv* (2025), *cond-mat.str-el*, 2506.02128.
- [59] Y.-H. Zhang, Holon metal, charge-density-wave and chiral superconductor from doping fractional Chern insulator and $su(3)_1$ chiral spin liquid, *arXiv* (2025), *cond-mat.str-el*, 2506.00110.